Latent Convergent Cross Mapping : Appendix

Anonymous Author(s)
Affiliation
Address
email

A Double pendulum

Figure 1 presents a graphical representation of a double pendulum with its two masses and two weightless rods. Figure 2 shows examples of trajectories generated by a double pendulum.

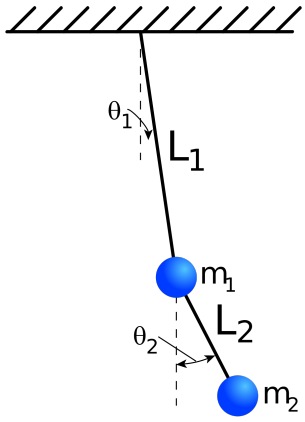

Figure 1: Physical representation of the double pendulum[1]

The double pendulum is a simple physically system that is chaotic and exhibits rich dynamical behavior. The Lagrangian of the double pendulum is

$$\mathcal{L} = \frac{1}{2}(m_1 + m_2)l_1^2\dot{\theta}_1^2 + \frac{1}{2}m_2 l_2^2\dot{\theta}_2^2 + m_2 l_1 l_2 \dot{\theta}_1\dot{\theta}_2\cos(\theta_1 - \theta_2). \tag{1}$$

The corresponding Hamiltonian can be derived using Legendre transform $H = \sum_i \dot{\theta}_i p_i - \mathcal{L}$.

The system evolution can be simulated by integrating the Hamilton equations:

$$\dot{\theta}_i = \frac{\partial H}{\partial p_i}$$
$$\dot{p}_i = -\frac{\partial H}{\partial \theta_i}$$

[1] Source: JabberWok / Wikimedia Commons, CC-by-3.0.

Submitted to 34th Conference on Neural Information Processing Systems (NeurIPS 2020). Do not distribute.

The Jacobian of the right hand side is

$$J = \begin{bmatrix} \frac{\partial^2 H}{\partial \theta_1 \partial p_1} & \frac{\partial^2 H}{\partial^2 p_1} & \frac{\partial^2 H}{\partial p_1 \partial \theta_2} & \frac{\partial^2 H}{\partial p_1 \partial p_2} \\ -\frac{\partial^2 H}{\partial^2 \theta_1} & -\frac{\partial^2 H}{\partial \theta_1 \partial p_1} & -\frac{\partial^2 H}{\partial \theta_1 \partial \theta_2} & -\frac{\partial^2 H}{\partial \theta_1 \partial p_2} \\ \frac{\partial^2 H}{\partial \theta_1 \partial p_2} & \frac{\partial^2 H}{\partial p_1 \partial p_2} & \frac{\partial^2 H}{\partial \theta_2 \partial p_2} & \frac{\partial^2 H}{\partial^2 p_2} \\ -\frac{\partial^2 H}{\partial \theta_1 \partial \theta_2} & -\frac{\partial^2 H}{\partial p_1 \partial \theta_2} & -\frac{\partial^2 H}{\partial^2 \theta_2} & -\frac{\partial^2 H}{\partial \theta_2 \partial p_2} \end{bmatrix}.$$

Note that the diagonal elements cancelling in pairs, which results in a trace of zero that indicates the volume-preserving property of the Hamiltonian flow according to Liouville's theorem. This property corresponds to information preservation in nondissipating physical systems. Consequently, a noncoupled double pendulum does not have a proper attractor. However, for a given initial condition, and thus given energy, the possible states still form a densely populated volume in state-space. Applying the nonphysical coupling term, the conservation rule do not hold anymore.

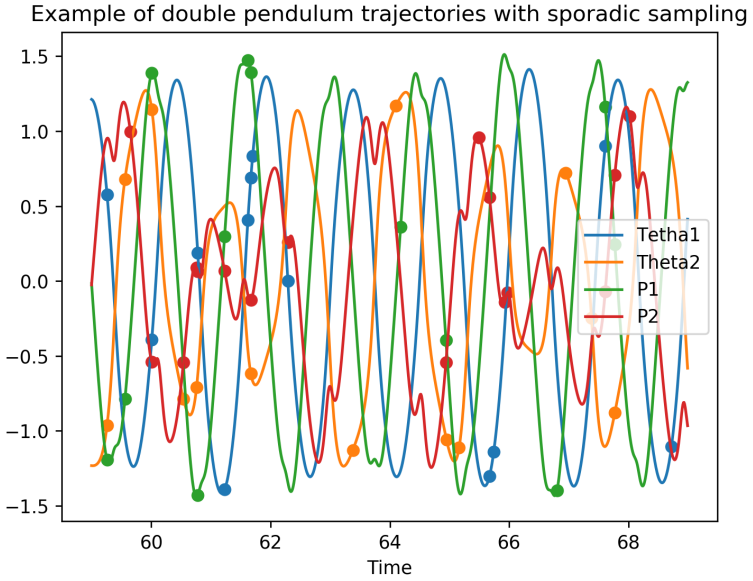

Figure 2: Example of trajectories generated by a double pendulum. The solid lines represent the true process and the dots the sampled measurements.

The real part of the eigenvalues of J are called the local Lyapunov exponents.

The direction of the largest expansion evolves as

$$\frac{d\mathbf{q}}{dt} = J\mathbf{q}$$
$$|\mathbf{q}(0)| = 1$$

The largest Lyapunov exponent is given by

$$\lambda_1 = \lim_{t\to\infty} \frac{1}{t} \log |\mathbf{q}(t)|.$$

Note that in stationary processes J is constant, and the differential equation have a closed form solution

$$\mathbf{q}(t) = \mathbf{q}(0)e^{Jt},$$

and the local and global Lyapunov exponents are equal.

The largest Lyapunov exponent can be described intuitively as

$$|\delta(t)| \approx |\delta(0)|e^{\lambda_1 t},$$

where $\delta(t)$ is defined as the difference between two phase-space trajectories, with initial condition infinitesimally close to each other:

$$\mathbf{x}'(t) = \mathbf{x}(t) + \delta(t), t \geq 0$$
$$|\delta(0)| \leq \epsilon.$$

We use numerical integration to compute the largest Lyapunov exponent of the double pendulum, and verify that it is in the chaotic regime.

Table 1: Parameters [m, kg] and the largest Lyapunov exponents of the uncoupled pendulums ($\lambda_1 > 0$ indicates chaotic behavior). We report means and their confidence interval over 10 repetitions with initial angles perturbed with $\sigma = 0.05$ normal distributed noise.

SYSTEM		l_1	l_2	m_1	m_2	θ_1	θ_2	λ_1 AND CI (80%)
$X \leftarrow Y$	X	1	0.5	2.0	1.0	1	-0.5	$0.306\,(0.149, 0.468)$
	Y	0.5	1.0	0.5	4.0	1	-0.5	$0.005\,(0.001, 0.010)$
	WHOLE $X \rightarrow Y$ SYSTEM							$0.318\,(0.183, 0.422)$
$X \leftarrow Z \rightarrow Y$	X	0.5	1.0	2.0	1.0	1.0	-0.5	$0.008\,(0.006, 0.009)$
	Y	0.5	1.0	2.0	1.0	1.0	-0.5	$0.008\,(0.006, 0.009)$
	Z	1.0	1.0	1.0	3.0	1.0	-0.5	$0.007\,(0.005, 0.008)$
	WHOLE $X \leftarrow Z \rightarrow Y$ SYSTEM							$0.090\,(0.027, 0.510)$

B Interacting neuron populations

The time series is the average membrane potential of two populations of leaky integrate-and-fire neurons with alpha-function shaped synaptic currents (*iaf_psc_alpha*) simulated by NEST-2.20.0 (Fardet et al., 2020). Each population contains 100 units with sparse random excitatory synapses inside population, and unidirectionally from population A to population B. A Poisson generator with rate of 40kHz was used to excite the network.

Table 2: Neuron populations. Every non-specified model parameter is left at the default value.

Population	tau_m [ms]	I_e [μA]
A	$\mathcal{U}(15.0, 16.0)$	0.0
B	$\mathcal{N}(15.0, 1.0)$	60.0
C (not obs.)	10.0	0.0

Table 3: Synapses. Parameters have been tuned to achieve stable firing without depolarizing the neuron populations.

From	To	connection type	parameter
Poisson	A	fixed outdegree	outdegree = 10
Poisson	C	fixed outdegree	outdegree = 10
A	A	fixed indegree	indegree = 67
B	B	fixed indegree	indegree = 20
C	C	fixed indegree	indegree = 67
C	B	fixed outdegree	outdegree = 60

In Figure 3, we plot the reconstruction correlations of the coupled neuron populations obtained with the fully observed time series (10 observations per second) and evaluated with standard CCM. We observe a small convergence in the reconstruction in the non-causal direction, indicating potential synchrony. As presented in Table **??**, our approach also captures this small reconstruction signal.

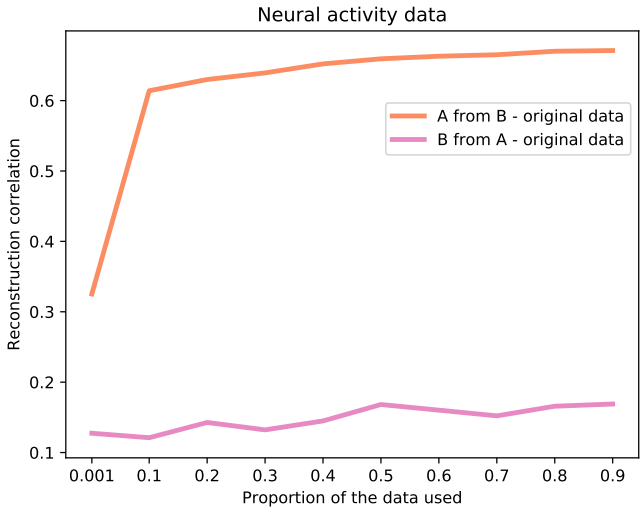

Figure 3: Result of CCM on fully observed neural activity data. Despite a clear signal of A driving B, we observe some positive correlation for the reconstruction in the noncausal direction.

C Results with univariate Gaussian Processes

In Table 4, we present the results of our experiments with univariate Gaussian Processes (GP). In this case, we only learn a GP on the dimension of interest to compute the delay embeddings. As we can see, results are slightly worse than when using multivariate Gaussian Processes (MVGP).

D Failure of the Granger causality framework

To show how the Granger causality framework fails in the general nonlinear dynamical systems case, we consider the following coupled dynamical system:

$$\begin{aligned} X[t+1] &= X[t](a - bX[t] - cY[t]) \\ Y[t+1] &= Y[t](d - eY[t]) \end{aligned}$$

Following Granger causality, including values of Y for predicting $X[t+1]$ should increase the prediction accuracy, and thus hint towards a causal effect of Y on X. However, dynamics of $X[t]$ can be rearranged such that all information about $Y[t]$ is contained in $X[t]$ already. Indeed,

$$Y[t] = \frac{-1}{c}\left(\frac{X[t]}{X[t-1]} - a + b\right)\left(d + \frac{e}{c}\left(\frac{X[t]}{X[t-1]} - a + b\right)\right).$$

Conditioning on $Y[t]$ would not bring additional information and Granger causality would then fail to uncover the right causal structure.

E Proof of Lemma 3.1

Proof. We first write the map $\Phi^k_{g(\phi_H),\alpha_H}(H(t))$ in its full form:

Table 4: Average reconstruction scores $\mathcal{S}_c$ (and their standard deviations) in all directions for the double pendulum and neural activity experiments. Standard deviations are computed using 5 repetitions. Significant correlations compared to noncoupled dynamical systems are in bold ($p < 0.01$). Significance is computed using the Mann-Whitney rank test. Our approach detects the correct causal structure. and highlight correct and wrong direction detection respectively.

DATA	SPATIAL CCM	GP	MVGP	LATENT-CCM
CASE 1				
$X \to Y$	-0.017 $\pm$ 0.037	0.002 $\pm$ 0.004	0.009 $\pm$ 0.014	0.001 $\pm$ 0.013
$\mathbf{X} \leftarrow \mathbf{Y}$	0.018 $\pm$ 0.0056	-0.001 $\pm$ 0.003	-0.001 $\pm$ 0.021	0.055 $\pm$ 0.001
$AUC_{1\to2}$	0.2 (P=0.98)	0.6 (P=0.22)	0.66 (P=0.11)	0.55 (P=0.35)
$AUC_{2\to1}$	0.6 (P=0.23)	0.44 (P=0.67)	0.44 (P=0.67)	**1 (P<0.001)**
CASE 2				
$X \to Y$	0.488 $\pm$ 0.074	-0.01 $\pm$ 0.008	-0.005 $\pm$ 0.009	0.001 $\pm$ 0.005
$X \leftarrow Y$	0.181 $\pm$ 0.119	-0.000 $\pm$ 0.003	-0.007 $\pm$ 0.012	0.009 $\pm$ 0.014
$X \to Z$	0.054 $\pm$ 0.021	-0.003 $\pm$ 0.003	-0.002 $\pm$ 0.014	0.035 $\pm$ 0.019
$\mathbf{Z} \to \mathbf{X}$	0.324 $\pm$ 0.197	0.061 $\pm$ 0.004	0.012 $\pm$ 0.014	0.657 $\pm$ 0.105
$Y \to Z$	-0.071 $\pm$ 0.078	-0.003 $\pm$ 0.003	-0.003 $\pm$ 0.023	0.005 $\pm$ 0.011
$\mathbf{Z} \to \mathbf{Y}$	0.101 $\pm$ 0.052	0.039 $\pm$ 0.008	-0.003 $\pm$ 0.016	0.555 $\pm$ 0.109
$AUC_{1\to2}$	**1.00 (P<0.001)**	0.21 (P=0.98)	0.31 (P=0.91)	0.78 (P=0.02)
$AUC_{2\to1}$	**1.00 (P<0.001)**	0.49 (P=0.53)	0.31 (P=0.92)	0.67 (P<0.09)
$AUC_{1\to3}$	**0.98 (P<0.001)**	0.35 (P=0.87)	0.61 (P=0.19)	0.79 (P=0.02)
$AUC_{3\to1}$	**0.93 (P<0.001)**	0.74 (P=0.03)	**0.81 (P=0.01)**	**1.00 (P<0.001)**
$AUC_{2\to3}$	0.26 (P=0.97)	0.36 (P=0.85)	0.45 (P=0.63)	0.46 (P=0.62)
$AUC_{3\to2}$	0.79 (P=0.02)	0.58 (0.26)	0.43 (P=0.69)	**1.00 (P<0.001)**
COUPLED				
$\mathbf{A} \to \mathbf{B}$	0.267 $\pm$ 0.001	0.028 $\pm$ 0.006	0.028 $\pm$ 0.006	0.295 $\pm$ 0.012
$A \leftarrow B$	0.055 $\pm$ 0.003	0.026 $\pm$ 0.010	0.026 $\pm$ 0.010	0.033 $\pm$ 0.012
$AUC_{A\to B}$	**1.00 (P=0.006)**	**1.00 (P=0.006)**	**1.00 (P=0.006)**	**1.00 (P=0.006)**
$AUC_{B\to A}$	**1.00(P=0.006)**	**1(P=0.006)**	**1.00(P=0.006)**	**1.00(P=0.006)**
INDEPENDENT				
$X \to Y$	-0.012 $\pm$ 0.001	-0.002 $\pm$ 0.008	-0.002 $\pm$ 0.008	-0.006 $\pm$ 0.007
$X \leftarrow Y$	-0.001 $\pm$ 0.001	-0.003 $\pm$ 0.005	-0.003 $\pm$ 0.005	-0.002 $\pm$ 0.008

$$
\begin{aligned}
&\Phi^k_{g(\phi_H),\alpha_H}(H(t)) : \mathcal{H} \to \mathbb{R}^k \text{ s.t.} \\
&\Phi^k_{g(\phi_H),\alpha_H}(H(t)) = (\alpha_H(g(\phi_{H,0}(H(t)))), \alpha_H(g(\phi_{H,-\tau}(H(t)))), ..., \alpha_H(g(\phi_{H,-k\tau}(H(t))))) \\
&\qquad = (\alpha_H(g(H(t))), \alpha_H(g(H(t-\tau))), ..., \alpha_H(g((H(t-k\tau))))) \\
&\qquad = (\alpha_H(X[t]), \alpha_H(X[t-\tau]), ..., \alpha_H(X[t-k\tau])),
\end{aligned}
$$

where the last line follows from the definition of the dynamical system. Φ then maps the latent process to the delay embedding of X obtained with observation function α_H.

As the observation function $\alpha_H \in \mathcal{C}^2$, the flow ϕ_H and the function $g(\cdot)$ are all continuous, this implies that the map Φ is also continuous in $H(t)$. It is also surjective as all delay embeddings (or points in the state-space) will have at least one latent value generating this delay embedding. Indeed, if we write $\mathcal{M}'_{\alpha_H}$ as the shadow manifold of the delay embeddings of X with observation function α_H, we have that

$$
\forall m \in \mathcal{M}'_{\alpha_H}, \exists h \in \mathcal{H} \text{ s.t. } \Phi^k_{g(\phi_H),\alpha_H}(h) = m.
$$

Let us now assume that there exists a specific observation function α^*_H such that Φ is injective. The map $\Phi_{\alpha^*_H}$ is then bijective. Furthermore, as both $\mathcal{H}$ and $\mathcal{M}'_{\alpha^*_H}$ are endowed with a metric, the map $\Phi_{\alpha^*_H}$ is a homeomorphism between $\mathcal{H}$ and $\mathcal{M}'_{\alpha^*_H}$.

We now show that Φ is a homeomorphism for any observation function. From Takens' theorem, any delay embedding with valid observation function α, dimension k, and delay τ is a valid embedding

of the strange attractor of the dynamical system. There must then exists a homeomorphic map Ψ between any two valid delay embeddings with different observation functions:

$$\forall \alpha, \beta \in \mathcal{C}^2, \mathbb{R} \to \mathbb{R}\ , \exists \text{ homeomorphism } \Psi_{\alpha,\beta} : \mathcal{M}'_\alpha \to \mathcal{M}'_\beta \text{ s.t.}$$
$$\forall m_\alpha \in \mathcal{M}'_\alpha, m_\beta \in \mathcal{M}'_\beta, \Psi_{\alpha,\beta}(m_\alpha) = m_\beta.$$

By transitivity, there is now a homeorphism between $\mathcal{H}$ and any valid delay embedding defined with observation function α_H defined as $\Psi_{\alpha^*_H,\alpha_H} \circ \Phi^k_{g(\phi_H),\alpha^*_H}(H(t))$. By Takens' theorem, $\mathcal{H}$ is thus an embedding of the strange attractor of the dynamical system containing $X[t]$.

□

References

Tanguy Fardet, Stine Brekke Vennemo, Jessica Mitchell, Håkon Mørk, Steffen Graber, Jan Hahne, Sebastian Spreizer, Rajalekshmi Deepu, Guido Trensch, Philipp Weidel, Jakob Jordan, Jochen Martin Eppler, Dennis Terhorst, Abigail Morrison, Charl Linssen, Alberto Antonietti, Kael Dai, Alexey Serenko, Binghuang Cai, Piotr Kubaj, Robin Gutzen, Hanjia Jiang, Itaru Kitayama, Björn Jürgens, and Hans Ekkehard Plesser. Nest 2.20.0, January 2020. URL `https://doi.org/10.5281/zenodo.3605514`.